Smart Mater. Struct. **6** (1997) 265–277. Printed in the UK PII: S0964-1726(97)82521-9

Modeling of a flexible beam actuated by shape memory alloy wires

Steven G Shu†, Dimitris C Lagoudas‡, Declan Hughes§ and John T Wen§

† Department of Mechanical Engineering, Aeronautical Engineering and Mechanics, Rensselaer Polytechnic Institute, Troy, NY 12180, USA
‡ Aerospace Engineering Department, Texas A&M University, College Station, TX 77843-3141, USA
§ Department of Electrical, Computer, Systems Engineering, Rensselaer Polytechnic Institute, Troy, NY 12180, USA

Received 5 February 1995, accepted for publication 14 February 1997

Abstract. A thermomechanical model is developed to predict the structural response of a flexible beam with shape memory alloy (SMA) wire actuators. A geometrically nonlinear static analysis is first carried out to investigate the deformed shape of a flexible cantilever beam caused by an externally-attached SMA wire actuated electrically. The actuation force applied by the SMA actuator to the beam is evaluated by solving a coupled problem that combines a thermodynamic constitutive model of SMAs with the heat conduction equation in the SMA and the structural model of the beam. To calculate the temperature history of the SMA actuator for given electrical current input, the heat transfer equation is solved with the electrical resistive heating being modeled as a distributed heat source along the SMA wire. The steps in the formulation are connected together through an iterative scheme that takes into account the static equilibrium of the beam and the constitutive relation of SMAs, thus translating an electrical current history input into beam strain output. The proposed model is used to simulate the experimental results, thus demonstrating the feasibility of using SMA actuators for shape control of active flexible structural systems.

1. Introduction

Active flexible structural systems will require improved structural performance to meet serious control issues. Active vibration suppression, precision pointing and shape control techniques have to be developed to accurately control and position large flexible structures in a changing environment. To meet these requirements, structural members, such as flexible beams, which may contain their own local sensors, actuators, and computational/control capabilities, need to be investigated (Akella *et al* 1994). The search for non-conventional materials used as actuators to satisfy control performance requirements becomes one of the main tasks. Shape memory alloys, due to their capability of large actuation force and displacement, have become a promising candidate during the last ten years (Duerig *et al* 1990) and have been proposed for use in a wide array of engineering structures. Rogers *et al* (1989) embedded SMA wires into composite plates to utilize the phase transformation as a means for altering the static deflection and modal characteristics of these plates. Lagoudas and Tadjbakhsh (1993) formulated in three dimensions a flexible rod with embedded line SMA actuators. Both the rod and the line actuator are assumed to be initially curved and relatively positioned in an arbitrary way. The deformed shapes of the rod under repeated thermal actuation and the resulting shape memory loss due to the development of residual stresses are evaluated.

However, the complexity of the applications of the composite plates and rods combined with the intricate nonlinear behavior of the SMA material itself makes analysis and design difficult. For this reason, we have chosen here to examine a simple cantilever beam actuated by an externally attached SMA wire actuator designed to exhibit the essential functions of the active structural system. External actuators have also better control authority since the actuator can be placed at different offset distances from the beam. The moment, caused by the actuation force from the externally line actuator, is much greater than that in a composite beam with an embedded line actuator along the beam and with the same magnitude of the actuation force. While the increase in the flexural stiffness of the beam with externally-attached SMA wire actuator is ignorable. Such a configuration also allows the introduction of fast convection cooling, which is very important in shape control applications that require a high-frequency response of SMA actuators.

There are several reported cases of using similar configurations of externally-attached SMA actuators. For example, Baz *et al* (1995) investigated the feasibility of

utilizing an externally-attached SMA in controlling the vibrations of a cantilever beam. The results demonstrated the potential of the SMA as a viable means of damping out the vibration of a beam. In that work, the actuation force of SMAs was assumed to be an exponential function of time, and was not derived from the constitutive relation of SMAs. Chaudhry and Rogers (1991) demonstrated the possibility of using this configuration to induce deflections of a beam and thus the feasibility of using this configuration for shape control. A fixed value of an attached load was used and there is no actual SMA material parameter involved. Brand *et al* (1994) discussed a solution of a flexible beam and a constitutive model of SMAs. However, it was found necessary to further investigates the solution procedure and the coupling between the beam and the SMA actuators was not included in that work. This work systematically investigates the strong coupling between the nonlinear solution of the large deflection problem of a flexible cantilever beam with a SMA constitutive model and electrical current control, in which the actuation force applied to the beam was actually from the SMA actuator. It thus demonstrated the ability of SMA actuators to be used for active shape control of a flexible structural system. Our corresponding experimental set-up was prepared by Akella *et al* (1994) to facilitate this study as shown in figure 1.

For the first part of the modeling, the flexible cantilever beam with an externally-attached SMA wire actuator is investigated. The beam equilibrium equation is obtained by simplification of the generalized three-dimensional (3D) rod theory proposed by Lagoudas and Tadjbakhsh (1992, 1993). An analytical solution of the nonlinear differential equation of the actuated beam is obtained, motivated by the 'elastica' solution given by Kirchhoff in 1859 (see Allen *et al* 1980, Bazant *et al* 1991). Because of the changing inclination angle of the load due to the actuating SMA, an additional unknown has to be introduced to the differential equation and thus an additional nonlinear equation has to be solved for this problem.

The thermomechanical constitutive theory of SMA is a key part of the system model. A 3D thermodynamic constitutive model has been developed by Boyd and Lagoudas (1994a) and modified by Bo and Lagoudas (1994b). This model has been used by Lagoudas *et al* (1994) for SMA actuators embedded in metal matrix composites where a multi-axial stress state exists. In the present paper, a one-dimensional (1D) simplification of the 3D model is used for predicting the thermomechanical response of the attached SMA actuator. The temperature distribution of the SMA is found by solving the 1D heat transfer equation, where the Joule heating is introduced as a distributed heat source; the heat capacity and the free heat convection coefficient of the SMA are modeled by temperature-dependent functions in this investigation. Finally, the thermal and structural problems coupled together through beam equilibrium and the temperature-dependent constitutive response of the SMA actuator lead to a set of nonlinear algebraic equations that are solved numerically for the SMA actuation force and the deflected beam geometry.

The presentation of the material is as follows. An electro-thermomechanical model of the structural system is given in section 2. It consists of four subsections: subsection 2.1 presents a brief account of the nonlinear beam formulation; 2.2 summarizes a 1D constitutive model for SMAs; 2.3 considers the thermal problem of SMA actuators; 2.4 discusses the solution procedure for the coupled structural system. Section 3 presents the simulation of the structural response together with the correlation with experimental results. Section 4 includes the discussion and some key conclusions.

2. Electro-thermomechanical modeling of a flexible beam with an externally attached SMA actuator

The current experimental beam set-up, shown in figures 1 and 2 (Akella *et al* 1994), is controlled by a single Nitinol SMA actuator mounted at the tip and at the foundation of the beam (though a second opposing SMA wire, shown in the graphs, may be added to the other side at a later stage). Before the SMA wire is attached to the beam, it is subjected to a tensile loading and unloading procedure in order to provide some fraction of detwinned martensite in the wire, i.e. the SMA wire is prestrained to a certain percentage of its original length. The wire is then attached to the beam either with or without prestress. When the wire is heated above the austenitic start temperature by passing an electrical current, the SMA attempts to contract to its original length, thereby applying an actuation force on the beam. The SMA alloy acts as an actuator transforming electrical energy into mechanical energy. As the actuator is cooled below the martensitic finish temperature, it is stretched back approximately to its prestrained length by virtue of the flexural rigidity of the beam. Repeated alternate heating, cooling and stretching of the SMA actuator results in cyclic contraction and expansion of the actuator. Accordingly, the beam acquires different deflected shapes for different levels of actuation of the SMA wires. To cause deflection to the opposite side, a second SMA wire may be added and actuated, after the first has been transformed into the compliant martensitic phase. With two or more attached actuators, a more complex deformed shape may be induced by selective actuation of the SMA wires.

A schematic drawing of the active structural system of the flexible cantilever beam is shown in figure 3. Only one SMA wire actuator at one side of the beam is actually actuated in this study, the other is not shown in this drawing. The SMA actuator is mounted on the beam as in figure 3 with offset distances d_1 at the tip and d_2 at the foundation. The increase of the offset distances will increase the beam deflection for a given load in the wire. The subsequent deformation of the beam will be described as a function of temperature as the SMA wire undergoes reverse and forward transformation upon heating and cooling.

As found in the experiments shown later in section 3, the full transformation of the SMA wire when heated above the austenitic finish temperature usually results in a large deformation of the beam and a geometrically nonlinear theory may be necessary. In the subsequent section, the nonlinear beam theory will be discussed for large

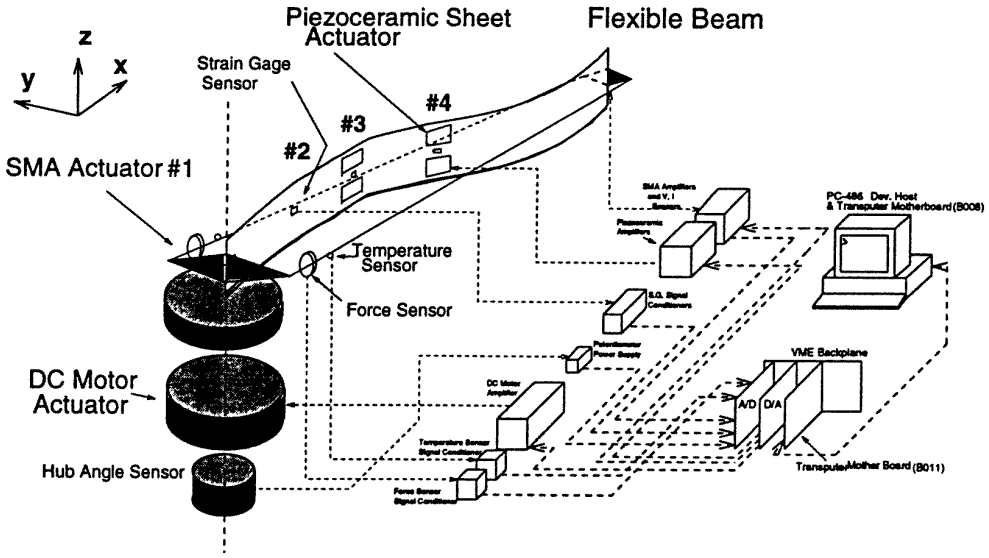

Figure 1. Experimental set-up of a cantilever beam with shape memory alloy actuators by Akella *et al* (1994).

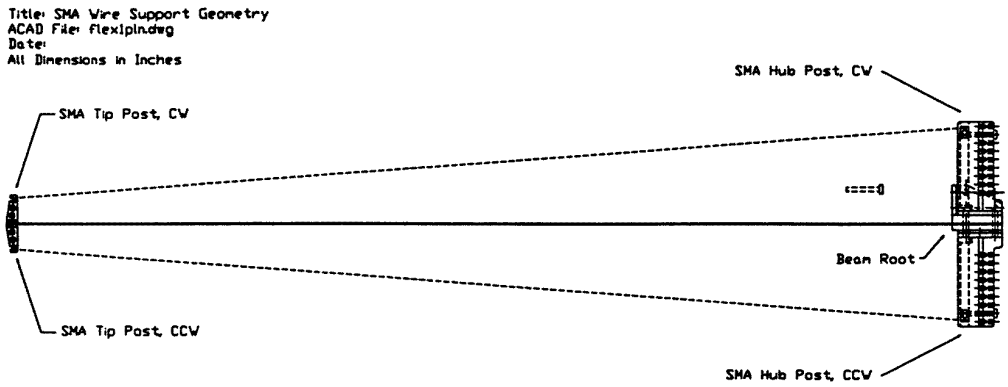

Figure 2. Plan view of the cantilever beam in figure 1 with shape memory alloy actuators.

deflections. The first step is to formulate the appropriate beam equations and then link those to SMA constitutive relations. The stress on the SMA wire is provided by the resistance to bending of the beam as the wire attempts to recover the original prestrain upon heating. Thus the load on the beam is caused by the stress in the wire. The stress and strain in the SMA wire are strongly coupled with the deformation of the beam. An iterative solution procedure needs to be carried out to solve this coupled system and this will be dealt with in section 2.4.

2.1. Nonlinear theory of a flexible beam with a wire actuator

The equilibrium equations for the 2D bending problem under consideration will follow from the 3D generalized formulation of a rod with an internally embedded SMA wire actuator by Lagoudas and Tadjbakhsh (1993). The simplified differential equations of equilibrium for the 2D bending problem with internally embedded SMA wire actuator are reproduced below from Lagoudas and Tadjbakhsh (1993).

$$\frac{\mathrm{d}F_2}{\mathrm{d}s} + \theta' F_1 + \theta' F^a = 0 \tag{1a}$$

$$\frac{\mathrm{d}F_1}{\mathrm{d}s} - \theta' F_2 + \frac{\mathrm{d}F^a}{\mathrm{d}s} = 0 \tag{1b}$$

$$\frac{\mathrm{d}M}{\mathrm{d}s} + (1+e)F_2 - d_0\frac{\mathrm{d}F^a}{\mathrm{d}s} = 0 \tag{1c}$$

where s is the arc length along the centroidal axis of the beam, $\theta' = \mathrm{d}\theta/\mathrm{d}s$ is the curvature of the beam due to bending and $\theta(s)$ is the rotation of the cross section of the beam at location s. F_1 and F_2 are the resultant forces in the beam at the location s along the direction of $\boldsymbol{e}_1$ and $\boldsymbol{e}_2$, respectively, for the 2D bending problem with the bending moment denoted by M. e is the elongation of the centroidal line of the beam. The internally embedded SMA wire actuator is parallel to the centroidal axis of the beam but it is offset by a distance d_0 from the centroidal axis. F^a is the actuation force on the beam due to an embedded SMA actuator. In our case, since there is no

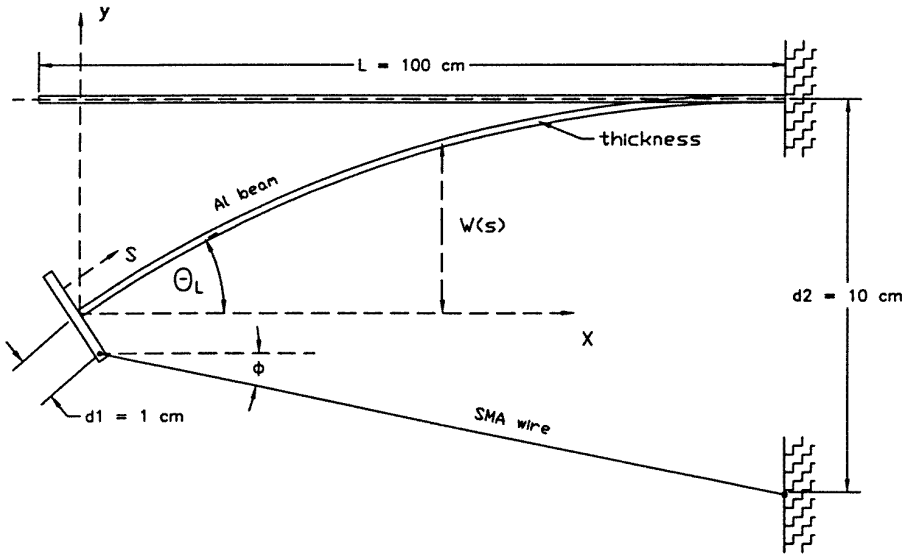

Figure 3. Schematic of flexible cantilever beam with a shape memory alloy wire actuator at one side of the beam.

internally embedded SMA actuator, $F^a = 0$. Thus the first two differential equations of (1) reduce to

$$\frac{d^2F_1}{d\theta^2} + F_1 = 0 \qquad \frac{d^2F_2}{d\theta^2} + F_2 = 0. \tag{2}$$

The solution of the above equations, after satisfying the boundary conditions, becomes

$$F_1 = -P_x \cos\theta + P_y \sin\theta$$
$$F_2 = P_x \sin\theta - P_y \cos\theta \tag{3}$$

where P_x and P_y are components of the actuation force P applied at the tip of the beam, i.e. $s = 0$, given by

$$P_x = P\cos\phi \qquad P_y = P\sin\phi \tag{4}$$

as shown in the free body diagram, figure 4, of the beam. In the above equation, ϕ is the inclination angle of the SMA wire, which is changing with the deflection of the beam. The geometric relation of the inclination angle is

$$\phi = \arctan\left[\frac{w_L + d_1\cos\theta_L - d_2}{L_b - u_L - d_1\sin\theta_L}\right] \tag{5}$$

where L_b is the centroidal arc length of the beam, w_L, u_L and θ_L are the tip deflection, horizontal displacement and rotation, respectively.

We also assume that the beam is inextensible, i.e. the elongation of the centroidal line. $e = 0$. After integrating equation (1c), and by taking into account equation (3) and the boundary condition $M(0) = -P_x d_1\cos\theta_L - P_y d_1\sin\theta_L$, the following equation is obtained:

$$M(s) + P_x[w(s) + d_1\cos\theta_L] - P_y[x(s) - d_1\sin\theta_L] = 0. \tag{6}$$

Using a linear constitutive relation between the curvature and the moment, i.e. $M(s) = EI\theta'$, the above equation reduces to

$$\theta' = -k^2\cos\phi[w(s) + d_1\cos\theta_L] + k^2\sin\phi[x(s) - d_1\sin\theta_L] \tag{7}$$

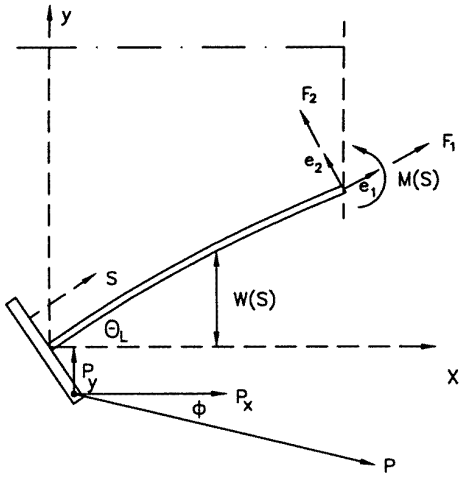

Figure 4. Free body diagram of deflected beam.

where $k = \sqrt{P/EI}$ and EI is the bending stiffness of the beam. The above equation is differentiated with respect to s, and it eventually becomes the differential equation to be solved for θ and ϕ

$$\theta'' = -k^2\cos(\theta - \phi) \tag{8}$$

with corresponding boundary condition at $s = 0$, from equation (7), given by

$$\theta'_L = -k^2 d_1\cos(\theta_L - \phi) \tag{9}$$

since $w(0) = 0$, $x(0) = 0$, and the boundary condition $\theta(L) = 0$ at $s = L$.

The following solution of the above boundary value problem is motivated by the solution of 'elastica' given by Kirchhoff in 1859 (Bazant *et al* 1991). If we express $\sin(\theta - \phi) = 2\sin[(\theta - \phi)/2]\cos[(\theta - \phi)/2]$,

multiply equation (8) by θ', and then, upon noting that $\theta'\theta'' = 1/2(\theta'^2)'$ we integrate (8) and take into account the boundary condition (9), we obtain

$$\frac{1}{4k^2}(\theta')^2 = -\sin^2\frac{\theta-\phi}{2} + m^2 \tag{10}$$

where $m^2 = (1/4)k^2 d_1^2\cos^2(\theta_L-\phi) + \sin^2[(\theta_L-\phi)/2]$. Taking the square root of equation (10) and noting that the rotation decreases as the beam arc length s increases, the minus sign of the square root is chosen. Integrating (10), we have the following integral:

$$-\int_{\theta(s)}^{0}\frac{\mathrm{d}\theta}{[m^2-\sin^2((\theta-\phi)/2)]^{1/2}} - 2k\int_s^L \mathrm{d}s = 0. \tag{11}$$

Introducing the variable change $\beta = \theta - \phi$, we obtain the following expression for $\theta(s)$ and ϕ:

$$-\int_0^{-\phi}\frac{\mathrm{d}\beta}{[m^2-\sin^2(\beta/2)]^{1/2}} + \int_0^{\theta(s)-\phi}\frac{\mathrm{d}\beta}{[m^2-\sin^2(\beta/2)]^{1/2}} - 2k(L-s) = 0. \tag{12}$$

Let $\theta(s) = \theta_L$ at $s = 0$ in the above expression, we obtain an equation to solve for the two unknowns of the tip rotation θ_L and the inclination angle ϕ. By introducing the additional change of variables, $m\sin\Phi = \sin\beta/2$, equation (12) can be rewritten as

$$f(\theta_L,\phi) = c_1F(m,\ \Phi_0) + c_2F(m,\ \Phi_L) - k(L-s) = 0 \tag{13}$$

with the standard incomplete elliptic integrals of the first and the second kind defined respectively by

$$F(m,\Phi_0) = \int_0^{\Phi_0}\frac{\mathrm{d}\Phi}{[1-m^2\sin^2(\Phi)]^{1/2}}$$

$$E(m,\Phi_0) = \int_0^{\Phi_0}[1-m^2\sin^2(\Phi)]^{1/2}\,\mathrm{d}\Phi \qquad 0 \le m < 1 \tag{14}$$

where Φ_0 and Φ_L are defined as

$$\sin\Phi_0 = \frac{1}{m}\frac{|\phi|}{2}$$

$$\sin\Phi_L = \frac{1}{m}\frac{|\theta_L-\phi|}{2} \tag{15}$$

and $c_1 = \mathrm{Sign}(\phi)$ and $c_2 = \mathrm{Sign}(\theta_L-\phi)$.

The deflection w_L and the horizontal displacement at the beam tip can be found by multiplying equation (11) by $\sin\theta$ and $\cos\theta$, respectively, and noting that $\mathrm{d}w = \sin\theta\mathrm{d}s$ and $\mathrm{d}u = \cos\theta\mathrm{d}s$. Following a similar procedure to that of equation (12) through (13) and integrating over the length of the beam s, the deflection at the beam tip can be found to be

$$w_L = \frac{1}{k}\sin\phi\{c_1[-F(m,\Phi_0)+2E(m,\Phi_0)] + c_2[-F(m,\Phi_L)+2E(m,\Phi_L)]\} - \frac{2m}{k}\cos\phi(-\cos\Phi_0+\cos\Phi_L) \tag{16}$$

while the horizontal displacement at the beam tip is given by

$$u_L = c_1F(m,\Phi_0) + c_2F(m,\Phi_L) - \frac{1}{k}\cos\phi\{c_1[-F(m,\Phi_0)+2E(m,\Phi_0)] + c_2[-F(m,\Phi_L)+2E(m,\Phi_L)]\} - \frac{2m}{k}\sin\phi(-\cos\Phi_0+\cos\Phi_L). \tag{17}$$

Note that in equation (13), the unknown $\theta(s)$ can only be solved after θ_L and ϕ are found. The two equations for θ_L and ϕ can be found by setting $\theta(0) = \theta_L$ in (13), thus obtaining the first nonlinear algebraic equation for θ_L and ϕ

$$f_1(\theta_L,\ \phi) = c_1F(m,\ \Phi_0) + c_2F(m,\ \Phi_L) - kL = 0 \tag{18}$$

and by substituting the expressions for w_L and u_L into the geometric relation (5), resulting in the second nonlinear algebraic equation for θ_L and ϕ:

$$f_2(\theta_L,\phi) = \phi - \arctan\left[\frac{w_L + d_1\cos\theta_L - d_2}{L_b - u_L - d_1\sin\theta_L}\right] = 0. \tag{19}$$

After solving for θ_L and ϕ from equations (18) and (19), the vertical and horizontal displacements can be obtained by equations (16) and (17). We are then able to solve for the rotations and deflections at any cross section of the beam. This is accomplished by solving equation (13) for θ_s once θ_L and ϕ are known. The strain of the beam at any location s can be found from equations (6) and (7), using the following expression

$$\varepsilon_s(s,y) = -\frac{M(s)}{EI}y = -\theta'(s)y = 2k\left[m^2-\sin^2\left(\frac{\theta(s)-\phi}{2}\right)\right]^{1/2}y \tag{20}$$

where y is the distance along the beam thickness from the centroidal axis of the beam.

Before the system response of the beam with the SMA actuator is investigated, the solution for the beam only, is carried out first. The two equations (18) and (19) of the nonlinear beam theory are solved for θ_L and ϕ simultaneously by using a Newton–Raphson method (Press *et al* 1986, IMSL Math/Library 1990). For this, P is assumed to be a known applied load, whose magnitude is constant while the inclination angle is still changing with the deflection of the beam. The comparison between the nonlinear solution provided above and the linear solution of the Euler–Bernouli beam with differential bending discussed in Liang and Rogers (1990) are shown in figure 5, for the material constants and geometry parameters given in table 1. Although both nonlinear and linear solutions agree well when the deflection of the beam is under 20% of its length, it is observed that the nonlinearity is significant when the deflection is large. Furthermore, care must be taken when using the linear beam theory since buckling may occur when the load P approaches a critical value (Liang and Rogers 1991). The corresponding deflection, to this critical value of the load, is about 20% of the beam length for this specific beam set-up.

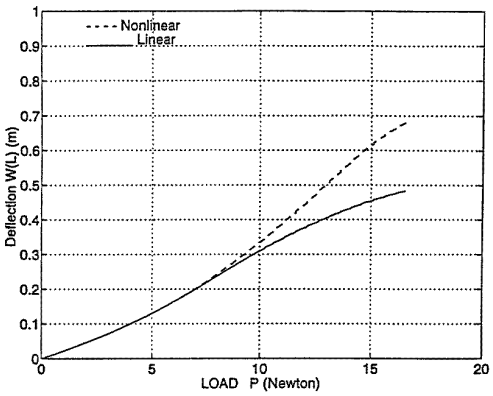

Figure 5. Comparison of nonlinear and linear beam theory for a flexible beam with an applied load at the beam tip, whose inclination angle is changing during loading.

Table 1. Material parameters and geometric constants of aluminum beam.

Parameter	Symbol	Value	Unit
Length	L_b	1.098	m
Width	w_b	0.103	m
Thickness	h_b	1.60×10^{-3}	m
Density	ρ_b	2.71×10^3	kg m^3
Young's modulus	E_b	68.95	Gpa
Offset distances	d_1	0.01	m
	d_2	0.10	m

2.2. Thermodynamic constitutive model of shape memory alloys

A brief outline of the 1D thermomechanical constitutive equation of the SMA wire used in this work is presented in this section. The thermodynamic constitutive model developed by Boyd and Lagoudas (1994a) and modified by Bo and Lagoudas (1994b) is used for predicting the thermomechanical response of the SMA. This model, originally formulated in 3D, is reduced for the purpose of this work to a 1D formulation.

The generalized Hooke's law takes the form

$$\sigma = E\varepsilon^e = E[\varepsilon - \varepsilon^t - \alpha(T - T_0)] \tag{21}$$

where σ, ε, ε^e and ε^t are the uniaxial stress, total strain, elastic strain and transformation strain, respectively; $E = E^A + \xi(E^M - E^A)$ and $\alpha = \alpha^A + \xi(\alpha^M - \alpha^A)$ are Young's modulus and the thermal expansion coefficient, respectively; both are assumed to obey the rule of mixtures and are functions of the current volume fraction ξ of the martensitic phase. E^A, E^M, α^A and α^M are the corresponding material properties for pure phases with superscript 'A' for Austenite and superscript 'M' for Martensite, respectively; T is the current temperature with T_0 being a reference temperature. The transformation strain rate is assumed to be given by the evolution law (Boyd and Lagoudas 1994a)

$$\dot{\varepsilon}^t = \Lambda\dot{\xi} \tag{22}$$

where Λ in one dimension is given by

$$\Lambda = \begin{cases} H\sigma/|\sigma| & \dot{\xi} > 0 \\ H\varepsilon^t/|\varepsilon^t| & \dot{\xi} < 0 \end{cases} \tag{23}$$

which provides the directions in which the transformation strains develop. For example, the transformation strain is going to develop along the direction of the stress during forward transformation ($\dot{\xi} > 0$), while it is going to develop along the opposite direction of the previous developed transformation strain during reverse transformation ($\dot{\xi} < 0$). H is the maximum axial transformation strain $(\varepsilon^t)_{max}$, $|\sigma|$ and $|\varepsilon^t|$ are the absolute values of the stress σ and the transformation strain ε^t, respectively, reduced from the corresponding 3D forms. Note that if the SMA wire is loaded under tension only, Λ is a positive constant equal to H.

By utilizing the first law of thermodynamics to describe the energy balance and the second law of thermodynamics to describe the energy dissipation during the phase transformation, the criterion for the onset of the phase transformation is given by (Boyd and Lagoudas 1994a)

$$\Phi = \sigma^{eff}\Lambda + \tfrac{1}{2}\Delta a^1\sigma^2 + \Delta\alpha\sigma(T - T_0) + \rho\Delta a^4 T - \frac{\partial f(\xi)}{\partial\xi} - Y^{**} = 0. \tag{24}$$

In the above, $\sigma^{eff} = \sigma - \rho b_2\varepsilon^t$, b_2 is the kinematic hardening parameter; $\Delta a^1 = 1/E^M - 1/E^A$ is the difference of the elastic compliances; $\Delta\alpha = \alpha^M - \alpha^A$ is the difference of thermal expansion coefficient; $\rho\Delta a^4$ is the difference of the entropy at the reference state; Y^{**} is the threshold value of transformation; $f(\xi) = \frac{1}{2}\rho b_1\xi^2$ provides the isotropic hardening term characterized by the isotropic hardening parameter b_1. The above criterion is valid for both reverse and forward transformation but with different values of the parameters $\rho\Delta a^4$, Y^{**}, b_1 and b_2, which accounts for the hysteresis of shape memory alloys. For the example concerned in the work, b_2 is taken to be zero. The parameters $\rho\Delta a^4$, Y^{**} and b_1 can be calibrated with the material properties of shape memory alloys as given below. For the forward transformation during cooling, $\rho\Delta a^4 = -C^M H$, $Y^{**} = -C^M H M_{0s}$ and $\rho b_1 = C^M H(M_{0s} - M_{0f})$. For the reverse transformation during heating, $\rho\Delta a^4 = -C^A H$, $Y^{**} = -C^A H A_{0f}$, and $\rho b_1 = C^A H(A_{0f} - A_{0s})$. In the above, C^M and C^A are the slopes of the curves of the stress versus temperature; M_{0s}, M_{0f}, A_{0s} and A_{0f} are the start and finish temperatures at zero stress, with 'M' and 'A' representing martensite and austenite, respectively.

A return mapping scheme may be used for the numerical implementation of equations (21), (22) and (24) in the general case (Ortiz and Simo 1986, Lagoudas *et al* 1994) under given increments of temperature T and total strain ε. According to this algorithm, the elastic predictor is calculated first. Then, an iterative procedure needs to be carried out in order to obtain the transformation corrector until convergence is achieved. Since Λ is constant in the 1D extentional case, equation (22) can be directly integrated to obtain $\varepsilon^t = \Lambda\xi$. Thus the martensitic volume fraction ξ can be determined as a function of temperature by solving the nonlinear algebraic equation $\Phi = 0$ in equation (24),

after substituting the expression of σ from equation (21). We may then use a Newton–Raphson method to solve the nonlinear algebraic equation $\Phi = 0$ for ξ. In this paper, we use the return mapping scheme instead, since it is computationally efficient and guaranteed to return to the transformation surface $\Phi = 0$ (Ortiz and Simo 1986).

The total strain of the SMA wire used in the above constitutive equations is given by

$$\varepsilon = \frac{L_{SMA} - L^0_{SMA}}{L^0_{SMA}} + H \tag{25}$$

where $L^0_{SMA} = [L_b^2 + (d_1 - d_2)^2]$ is the original length of the SMA actuator if the horizontal position of the beam is taken as the initial state, such as in the case in which the cyclic thermomechanical loading starts at the martensitic state at low temperature. Note that the transformation strain ε^t at such initial state is taken to be the maximum prestrain H. L_{SMA} is the deformed length of the SMA actuator determined by the deformation of the beam

$$L_{SMA} = [(L_b - u_L)^2 + (w_L + d_1 - d_2)^2] \tag{26}$$

where u_L and w_L are given by equations (16) and (17).

2.3. Heating and cooling of shape memory alloy actuators

In the phase transformation function (equation (24)) of the constitutive model of the SMA, both the stress and temperature are the driving forces of phase transformation.

In general shape control applications, the SMA wire temperature is provided by either the surrounding medium, such as a hot water bath, or resistive heating with electrical current. In either case the temperature of the SMA is the control parameter, which can be solved from a heat transfer problem of a thin cylinder. In this section, the heat transfer problem of a thin wire actuator of the SMA with resistive heating in surrounding air is investigated.

The governing equation for the 1D heat conduction problem of a SMA wire is (Kakac *et al* 1987)

$$C_v(T)\frac{\partial T(x,t)}{\partial t} = k\frac{\partial^2 T(x,t)}{\partial x^2} - \frac{4h(T,D)}{D}[T(x,t) - T_\infty] + \rho_e J^2 \tag{27}$$

where $T(x,t)$ is the temperature at the location x at time t, k is the thermal conductivity and D is the diameter of SMA wire. The heat convection coefficient $h(T,D)$ is the rate of convective heat transfer occurring in the ambient temperature T_∞ along the sides of the SMA wire; ρ_e is the electrical resistivity and J is the magnitude of the current density; $C_v(T)$ is the heat capacity. If all material properties are assumed to be constants, we can solve this equation analytically with the boundary conditions $T(0,t) = T_1$, $T(L,t) = T_2$ for $t \geq 0$ and the initial condition $T(x,0) = T_0$ for $0 < x < L$ at $t = 0$.

The solution of equation (27) is shown in figure 6 for the given material parameters in table 2 under the conditions $T_2 = T_1 = T_0 = T_\infty$. It can be seen that the temperature distribution is uniform along the length of the wire except at the two ends. For the long wire used in this specific case, we may treat the wire to be of infinite length so that the end effect can be ignored. Thus the problem will be the same as the one with insulated boundary conditions at two ends, i.e. $\partial T(0)/\partial x = \partial T(L)/\partial x = 0$. The problem is then simplified to the following:

$$C_v(T)\frac{\partial T(t)}{\partial t} = -\frac{4h(T,D)}{D}[T(t) - T_\infty] + \rho_e J^2 \tag{28}$$

The heat capacity $C_v(T)$ is generally a temperature-dependent parameter, which characterizes the latent heat change and indicates the exothermic nature of the forward transformation and the endothermic nature of the reverse transformation. The heat capacity of a typical Ni–Ti SMA has been experimentally determined by Jackson *et al* (1972). Bhattacharyya *et al* (1995) proposed an empirical relation describing the dependence of C_v on T as follows,

$$C_v = C_v^0 + q\frac{\ln(100)}{|M_{0s} - M_{0f}|} \times \exp\left[-\frac{2\ln(100)}{|M_{0s} - M_{0f}|}\left|T - \frac{M_s + M_f}{2}\right|\right] \quad M_f \leq T \leq M_s \tag{29}$$

for the forward transformation and

$$C_v = C_v^0 + q\frac{\ln(100)}{|A_{0s} - A_{0f}|} \times \exp\left[-\frac{2\ln(100)}{|A_{0s} - A_{0f}|}\left|T - \frac{A_s + A_f}{2}\right|\right] \quad A_s \leq T \leq A_f \tag{30}$$

the reverse transformation. $q = 0.0618$ J mm^{-3}, a constant representing the total latent heat in the course of transformation. It can be determined experimentally by, say, a differential scanning calorimetric (DSC) measurement. The electrical resistivity ρ_e is taken to be constant. Even though ρ_e is also a function of temperature (Jackson *et al* 1972), the lack of reliable data prevents us from exploring this possibility in this work.

The free heat convection coefficient for a horizontal cylinder is usually a function of the surface temperature and the diameter of the cylinder (Kreith *et al* 1980)

$$h_c(T,D) = \frac{k}{D}Nu \tag{31}$$

where k is the thermal conductivity of the surrounding air and D is the diameter of SMA wire. Nu is the average Nusselt number for free convection of a horizontal cylinder or a wire (see the appendix).

2.4. Solution procedure

As discussed in section 2.1, when P is the known applied load, whose magnitude is constant while the inclination angle ϕ is still changing with the deflection of the beam, the problem can be solved by finding the roots of two equations (18) and (19) of nonlinear beam theory for θ_L and ϕ:

$$f_1(P, \theta_L, \phi) = c_1 F(m, \Phi_0) + c_2 F(m, \Phi_L) - kL = 0 \tag{18}$$

Table 2. Material parameters of shape memory alloy actuators.

Parameter	Symbol	Unit	Value	
			Case 1	Case 2
Length	L^0_{SMA}	m	1.10	1.10
Diameter	D	m	2.03×10^{-4}	2.03×10^{-4}
Young's modulus[a]	E^A	Gpa	69.00	69.00
	E^M	Gpa	30.00	30.00
Thermal expansion	α^A	1/°C	11.0×10^{-6}	11.0×10^{-6}
coefficient	α^M	1/°C	6.6×10^{-6}	6.6×10^{-6}
Poisson's ratio	μ	—	0.33	0.33
Density	ρ	kg m^3	2.71×10^3	2.71×10^3
Slope of stress	C^A	Mpa/°C	6.5	9.0
versus temperature plot	C^M	Mpa/°C	6.5	7.0
Transformation	A_{0s}	°C	66.0	48.0
temperatures[b]	A_{0f}	°C	83.0	53.0
	M_{0s}	°C	49.0	41.0
	M_{0f}	°C	33.0	31.5
Maximum transformation strain of SMA	H	—	5.5%	1.88%
Heat capacity	C^0_v	J m^{-3} °C	5.44×10^6	5.44×10^6
Electrical resistivity	ρ_e	Ω m	102.0×10^{-8}	102.0×10^{-8}

[a] '*A*' and '*M*' represent austenitic and martensitic phases, respectively.

[b] Subscripts *s* and *f* represent start and finish temperature with '0' standing for stress free state.

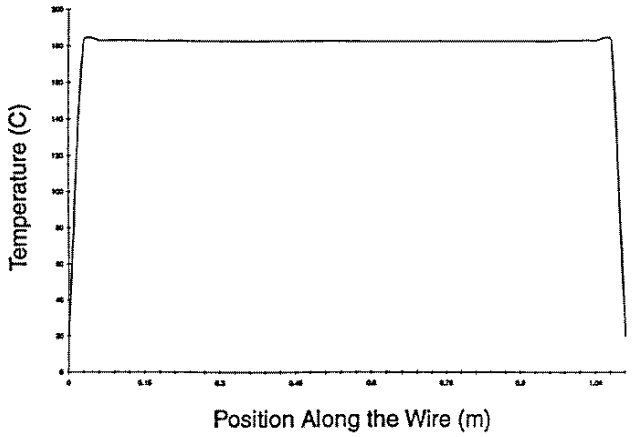

Figure 6. Temperature distribution along the shape memory alloy wire predicted by heating equation (27).

$$f_2(P, \theta_L, \phi) = \phi - \arctan\left[\frac{w_L + d_1 \cos\theta_L - d_2}{L - u_L - d_1 \sin\theta_L}\right] = 0. \tag{19}$$

However, when the force P is due to the actuation of SMA wire, it is not known in advance, and the above two equations become functions of P, θ_L and ϕ. There are now three unknowns and an additional equation is needed to solve for them.

The actuation force P is actually the result of the coupling effect between the shape memory effect and beam deformation. The coupling effect can be described as follows: after the SMA wire is prestrained and attached on the structure while still being in the martensitic state, it is actuated by resistive heating, i.e. passing an electrical current through the SMA wire. Once the temperature of the SMA wire exceeds the austenitic start temperature, the wire starts to contract to its memorized length that it had before prestrain. Since the SMA wire is constrained by the beam, a stress will be generated in the wire, which, in turn, applies a force P on the beam and causes the beam deflection. The stress of the SMA wire will be balanced by the force P at the conjunction of the wire and the beam. This equilibrium condition can be expressed as

$$f_3(P, \theta_L, \phi) = P - \sigma(\theta_L, \phi)A = 0 \tag{32}$$

where σ and A are the stress and cross sectional area of the SMA wire, respectively. Equation (32) is a function of P, as well as the beam tip rotation θ_L and the inclination angle ϕ, through the dependence of σ on them. The above three equations are solved simultaneously for P, θ_L and ϕ by using the Newton–Raphson method (IMSL Math/Library 1980, Press *et al* 1991). It is noted that the current stress σ

of the SMA is itself an implicit function of θ_L and ϕ, since the stress needs to be updated by the constitutive relations (21), (22) and 24) once the total strain ε is updated by equation (25), which is evaluated at the currently deformed shape of the beam characterized by θ_L and ϕ.

Now the general solution procedure can be briefly described as follows. Under the input electrical current density history $J(t)$, the temperature $T(t)$ of the SMA actuator can be obtained from equation (28). Once the temperature $T(t)$ at the current time t_i exceeds the austenitic start temperature A_s, the M $\rightarrow$ A phase transformation in the SMA is initiated and the constitutive relations (21), (22) and 24) are evaluated to obtain the current stress σ of the SMA. Then, the force P, the rotation θ_L and the inclination angle ϕ are found simultaneously by solving the three nonlinear equations (18), (19) and (32), using the Newton–Raphson method. Once P, θ_L and ϕ are updated, the total strain ε is updated by equation (25) and thus the current stress σ of SMA wire is also recalculated by the constitutive relations (21), (22) and (24). Thereafter, the load P, the rotation θ_L and the inclination angle ϕ are updated again by solving equations (18), (19) and (32). This iterative procedure stops once it reaches convergence and the next time $t_{i+1} = t_i + \Delta t$ is considered with the incremental time Δt. Once the values of P, θ_L and ϕ are evaluated, the beam response, such as the horizontal displacement u_L, the deflection w_L at the beam tip and the beam strain ε_s, can be found by equations (17), (16) and (20).

3. Simulation of structural response

The geometry of the aluminum beam to be investigated in this study and the pertinent material parameters are given in table 1. The material parameters of the SMA actuator are given in table 2. Cases 1 and 2 correspond to two different sets of SMA materials from Dynalloy, Inc (see reference). Case 1 is used for parametric study, while case 2 corresponds to the SMA materials actually used for the experiment.

For the static problem, the time response of the structural system, given electrical current input, is determined by the characteristic time of the SMA actuator, which is defined as the ratio of the heat capacity C_v over the heat convection term $4h/D$. Although the characteristic time of the SMA is the same in magnitude during both heating and cooling for the same heat convection coefficient, the cooling rate is much smaller than the heating rate. This is because heating is mostly controlled by the magnitude of the Joule heating term, while the cooling rate depends only on heat convection and the temperature difference between the actuator and the ambient temperature. Thus forced convection is used in this case to accelerate cooling. Under the on–off current input shown in figure 7, the corresponding temperature profile is shown in figure 8 (material of case 1, the same for figure 9) with a natural free convection coefficient $h = 1.5$ (W/m^2/K) during heating and a forced convection coefficient $h = 150$ (W/m^2/K) during cooling. However, the cooling rate is still much slower than that of heating. According to figures 8 and 9, it takes about 3.4 s to heat up to the austenite finish temperature $A_f = 122\,^\circ$C at stress $\sigma_{SMA} = 270$ Mpa and about 6 s to cool down to martensitic finish temperature $M_{0f} = 33\,^\circ$C.

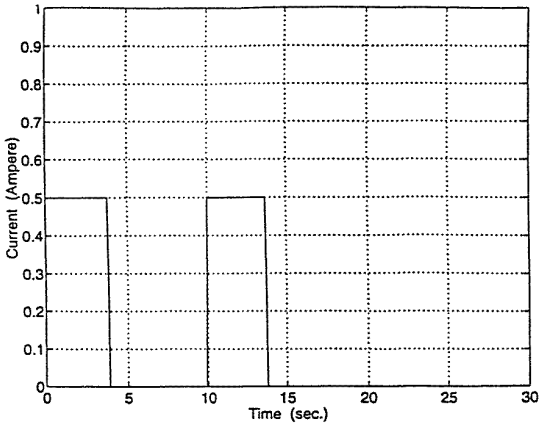

Figure 7. On–off step input of the electrical current profile used for the investigation of the structural response of the flexible beam with the SMA actuator.

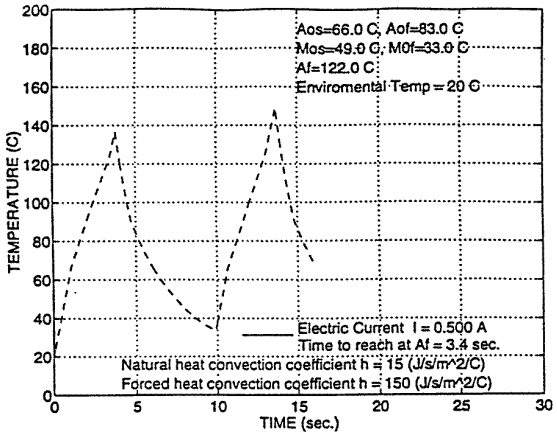

Figure 8. Temperature profile of a shape memory alloy actuator under the step input of figure 7 with h = 1.5 (W/m^2/K) for heating and h = 150 (W/m^2/K) for cooling.

The corresponding stress of SMA versus time under the electrical current input of figure 7 is shown in figure 9. Note that the relationship between SMA stress and time is approximately piecewise linear. A similar type of piecewise linear relationship also exists between stress and temperature in SMA wire as shown in figure 13(a), later. These results agree with the experimental results used in the paper by Rhee and Koval (1993), where a linear relationship between actuation force and temperature is used for a structural control strategy. It is important to mention that even though the structural response with the SMA actuator is approximately piecewise linear, the overall response exhibits strong hysteresis as seen in figures 13(a) and (b). We are currently investigating the impact of such hysteric response to the control strategy for shape control applications.

The temperature profiles for the SMA actuator under different heating rates due to different step inputs of

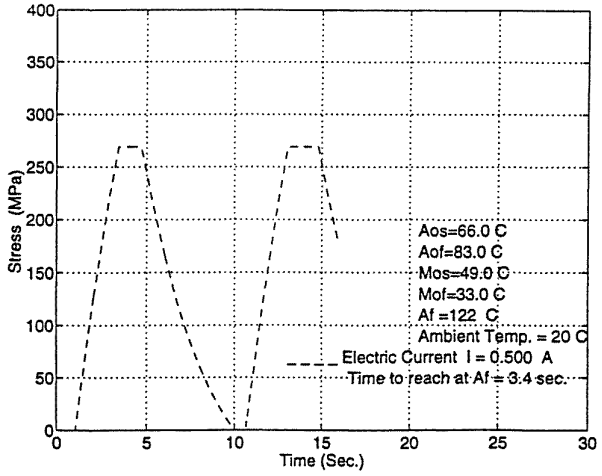

Figure 9. Time versus stress in a shape memory alloy actuator under the step input of figure 7.

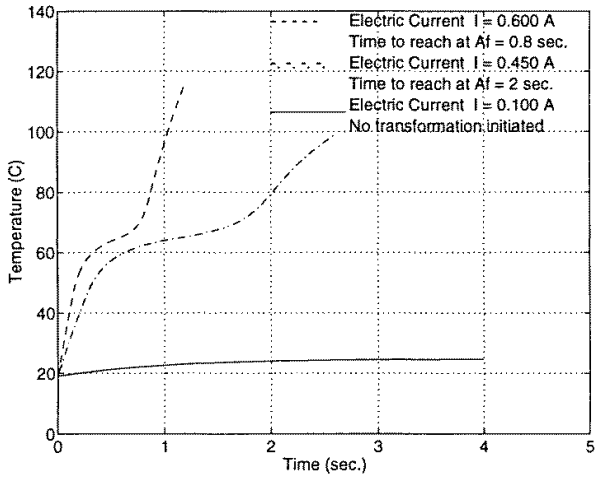

Figure 10. Predicted temperature profiles of a shape memory alloy actuator under different heating rates due to different step input of the electric current.

electrical current are shown in figure 10 (material of case 2, the same for the following figures). For example, under the current of 0.600 A, the time to reach the austenite transformation finish temperature takes less than 0.8 s. While under a current of 0.450 A, it takes about 2.0 s to finish the transformation. If the input current is too low to balance the heat loss due to convection, the transformation may not be completed or even initiated, which is the case with a current level of 0.100 A.

Finally, the structural response due to a ramp input of electrical current shown in figure 11 is investigated. In the experiments, the electric current shown in figure 11 is the controlled parameter. A miniature thermocouple ($\approx$0.114 mm bead diameter) is bonded to the SMA wire (0.152 mm diameter) by a thin (0.127 mm thick) strip of self-adhesive heat conductive elastomer (electrically insulating) and is used to measure a temperature (shown in figure 12) that approximates that of the SMA wire itself. A small inline load cell measures the SMA wire tension (shown in figure 13(a)), and a strain gage on the beam

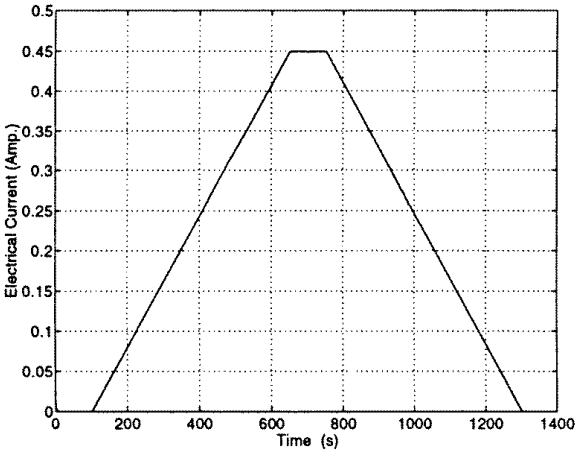

Figure 11. Ramp input of the electrical current profile for figures 13.

measures the induced beam strain (shown in figure 13(b)). A semiconductor thermometer was used to record the ambient temperature.

Figure 12 shows the simulated temperature profiles and that of the experiment due to the ramp input of electrical current shown in figure 11. The simulated curve is from equation (28) along with equations (29)–(31). The *Nusselt* number is determined by equation (A1) in the appendix. In the original formulation of equation (A1) provided by Kakac *et al* (1987). The constants α_1 and α_2 are $\alpha_1 = 0.60$ and $\alpha_2 = 0.387$, respectively, which are valid for a very wide range of Ra for cylinders ($10^{-5} \leq Ra \leq 10^{12}$). However, it is found that the *Rayleigh* number $Ra = GrPr$ for our very thin SMA wire used in the experiment is less than 10^{-5}, which is out of the above range. Nevertheless, we have still used the form of equation (A1) and identified the constants α_1 and α_2 in the Nusselt number of equation (A1) based on our temperature measurement shown in figure 11. It is estimated that $\alpha_1 = 1.00$ and $\alpha_2 = 0.287$ for the very thin SMA wire actuators used in this study. Figure 12 shows a good correlation between the model and the experiment for both low and high temperatures. It is noted that several factors may influence the accurate estimation of the constants α_1 and α_2, in particular, the exact knowledge of the resistivity ρ_e, which is taken as a constant in this study from Dynalloy, Inc (see reference). The subject of complete parameter identification for this system is currently under investigation.

The force–temperature hysteretic curve predicted by the model and that obtained from the experiment of the beam structural system under the ramp input current of figure 11 are shown in figure 13(a), whereas the strain–temperature curves are shown in figure 13(b). The strains are those at a distance $s = 0.824$ m from the beam tip.

The maximum transformation strain, i.e. the prestrain measured in the experiment, is 1.88%, which is the parameter H entered into the model. In the model prediction, the stress-free transformation temperatures, including the austenitic start and finish temperature A_{0s}, A_{0f}, the martensitic start and finish temperature M_{0s}, M_{0f}

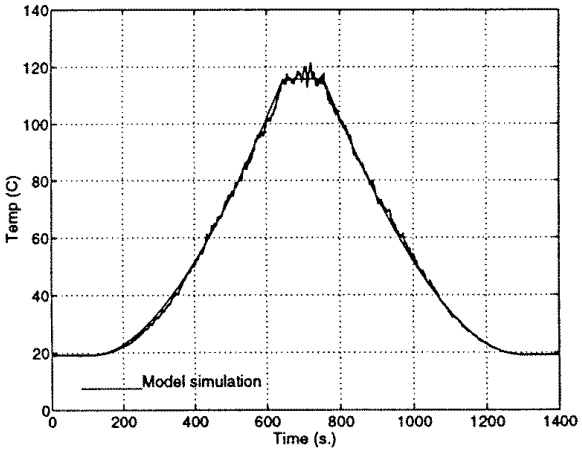

Figure 12. Comparison of temperature profiles with experiment under ramp input of the electrical current of figure 11. The model predicted curve is from equation (28) along with equations (29)–(31).

and the corresponding slopes C_A, C_M of the stress versus the temperature of the SMA actuator, are needed (see the details in Bo and Lagoudas (1994)). Those parameters can be obtained from the SMA wire test. The SMA wire used in the experiment contained nominally equal atomic weight (a 50%/50% ratio) of nickel and titanium. These wires were purchased from Dynalloy, Inc (see reference). Some of the parameters used in the model are provided by the company with listed data. However, the parameters relevant to the phase transformation are provided by the company in the form of experimental curves with large scattering in the data. It is known that the parameters of the phase transformation, for example, the stress-free transformation temperatures, are extremely sensitive to the composition and the processing of the alloy (Jackson *et al* 1972). Thus, we decided to identify the parameters relevant to the phase transformation from our experiment of the beam structure with the SMA actuator, by comparing the experimental data of figure 13(a) with the model simulation. While this can be done using established numerical procedures of system identification, we identified the parameters by a simple method of trial and error for the current problem. These parameters, A_{0s}, A_{0f}, M_{0s}, M_{0f}, C_A and C_M, have been given in table 2 (case 2). With these parameters, the strain–temperature hysteritic curve is predicted, as shown in figure 13(b). Note that although the SMA actuator is heated above the austenitic finish temperature A_f, the actuation force–temperature path reaches saturation at A_f. Since no more martensitic phase can be transformed into austenite when the temperature A_f is reached, the SMA wire recovers its initial prestrain, and a further increase in temperature does not induce any additional actuation force.

In closing, it is observed that the main features of the hysteresis, such as the maximum actuation force and the maximum strain of the beam, agree well with the experimental results. Other features, such as the austenitic finish temperature A_f and the martensitic start temperature M_s, can also be captured by the thermodynamic model, while near the austenitic start temperature and

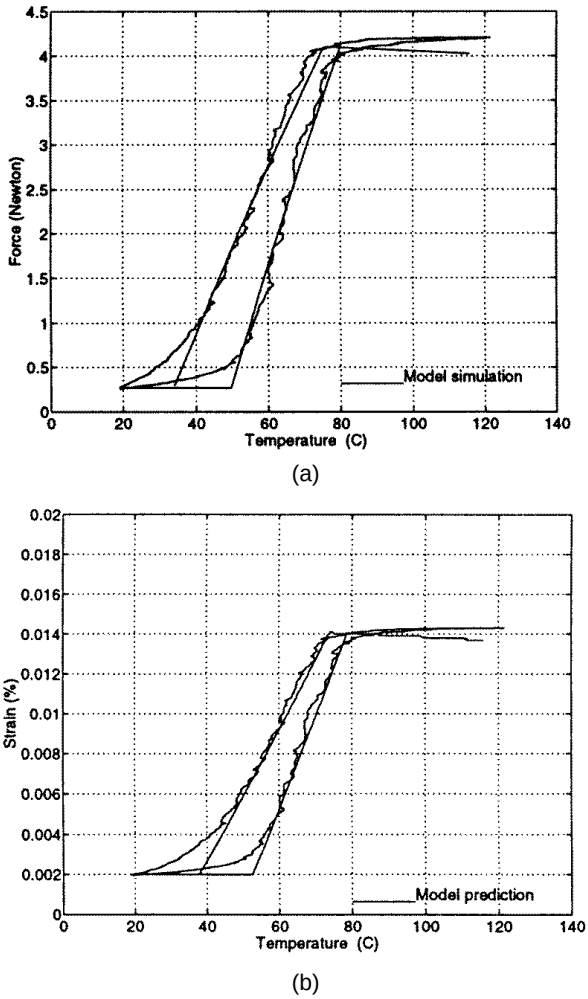

Figure 13. Hysteresis of the beam structure system: (a) force versus temperature of the SMA actuator, and (b) strains on the beam versus temperature of the SMA actuator, under the ramp input of current of figure 11.

martensitic finish temperature, the experimental curves in figures 13(a) and (b) show a more gradual variation than the curves from the model. We are currently implementing a modified constitutive model of SMAs based on a statistical distribution for the phase transformation temperatures (Bhattacharyya and Lagoudas 1995) that will account for the gradual phase transformation.

4. Conclusions

An electro-thermomechanical model was developed to simulate a shape memory alloy (SMA) wire-actuated compliant beam structure. A geometrically nonlinear analysis was first carried out to investigate the deformed shape of a flexible beam with a SMA wire actuated electrically. It was found that for this specific case, when the tip deflection of the beam is less than 20% of its length, an approximate linear beam model is appropriate, allowing the use of linear beam theory in modeling the dynamic structural response of the beam. However, for large deflections that may occur during the model prediction

and identification process, where the full transformation range of the SMA is triggered, the nonlinear beam theory is still necessary to correctly calibrate the model. An additional advantage of the nonlinear theory is that it is valid for applied loads larger than the critical buckling load, which is the limit load for the linear theory.

The actuation force applied by the SMA actuator to the beam was evaluated by using a thermodynamic constitutive model for SMAs. The temperature history in the SMA actuator for given electrical current input was evaluated by solving the heat conduction equation in the SMA actuator with the electrical resistive heating being modeled as a distributed heat source. Finally, the models used for the beam and the SMA actuator were connected through an iterative scheme that takes into account the static equilibrium of the beam, thus translating an input electrical current history into a beam strain output. The integrated modeling of the structural system has the following merits. (a) It gives physical models for each functional element of the structure and helps to understand the relationships among them. (b) It shows the influence of the material and geometrical parameters on the structural response. (c) It provides a basis for developing models suitable for structural analysis and control.

Good agreement of model simulation and experimental data for a flexible beam with an SMA actuator has been observed during cyclic heating and cooling of the SMA actuator. If the model is fully identified, it can be used to analyze the structural response of the system under any electrical current input, in particular the hysteric response due to SMA actuator hysteresis, which could facilitate the implementation of a structural shape control strategy.

Acknowledgment

The authors acknowledge the financial support of the Army Research Office, contract No DAAL03-92-G-0123, monitored by Dr G L Anderson.

Appendix A. Nusselt number for free convection of a horizontal cylinder or a wire

On the basis of numerous experiments it has been found that, for cylinders of small diameter, the average Nusselt number Nu can be related to the *Rayleigh* number, Ra, which is the product of the Grashof number Gr and the Prandtl number Pr, i.e. $Ra = GrPr$. In engineering practice, the average Nusselt number Nu is generally given in terms of the Rayleigh number Ra. The horizontal cylinder has been of interest to several investigators. Recently, Churchill and Chu (1975) have given a correlation covering a very wide range of Ra for isothermal cylinders (Kakac *et al* 1987, Kreith and Black 1980),

$$Nu = \left[\alpha_1 + \alpha_2 \left\{ \frac{GrPr}{[1 + (0.56/Pr)^{9/16}]^{16/9}} \right\}^{1/6}\right]^2 \quad \text{for } 10^{-5} \le Ra \le 10^{12}. \tag{A1}$$

Note that Nu and Ra are based on the current surface temperature T and the diameter D of the cylinder. The constants α_1 and α_2 can be correlated with experimental temperature measurements of very thin wires of shape memory alloys.

The Grashof number Gr and the Prandtl number Pr are given as (Morgan 1975, Churchill and Chu 1975)

$$G_r = \beta(T - T_\infty)\frac{gD^3}{\nu^2} \tag{A2}$$

$$P_r = \frac{\mu C_p}{k} \tag{A3}$$

respectively. In the formulas, $\beta = 1/T_{avg}$; $T_{avg} = (T + T_\infty)/2$; $g = 9.8$ m s^{-2} is the gravitational acceleration; ν is the kinematic viscosity; C_p is the heat capacity at constant pressure; μ and k are the viscosity and the thermal conductivity of the surrounding air, respectively. Note that the temperature at the wire surface T can be taken as the temperature of the wire for such a thin wire.

It is often necessary to iterate on the Grashof number and the Prandtl number since the temperature in Gr and Pr may not be explicitly known and all physical properties should be evaluated at the average temperature $T_{avg} = (T + T_\infty)/2$. The various physical parameters used in Grashof and Prandtl numbers are obtained by interpolation from table G.1 of Kreith and Black (1980).

References

Akella P, Chen X, Cheng W, Hughes D and Wen J 1994 Modeling and control of smart structures with bonded piezoelectric sensors and actuators *J. Intell. Mater. Syst. Struct.*

Allen H G and Bulson P S 1980 *Background to Buckling* (New York: McGraw-Hill)

Baz A, Imam K and McCoy J 1995 Active vibration control of flexible beams using shape memory actuators *J. Sound Vib.* **140** 437–56

Bazant Z P and Cedolin L 1991 *Stability of Structures—Elastic, Inelastic, Fracture, and Damage Theories* (Oxford: Oxford University Press)

Bhattacharyya A and Lagoudas D C 1995 A stochastic thermodynamic model for the gradual thermal transformation of SMA polycrystals *Smart Mater. Struct.* submitted

Bhattacharyya A, Lagoudas D C, Wang Y and Kinra V K 1995 On the role of thermoelectric heat transfer in the design of sma actuators: theoretical modeling and experiment *J. Intell. Mater. Struct.* at press

Bo Z and Lagoudas D C 1994a Deformations and thermal response of active flexible rods with embedded SMA actuators *Proc. SPIE* **2190** 495–505

Bo Z and Lagoudas D C 1994b Comparison of different thermodynamic models for shape memory alloys *Adaptive Structure and Composite Materals, Analysis and Applications* AD-vol 45, MD-vol 54, ed E Garcia, H Cudey and A Dasgupta (ASME) pp 9–19

Boyd J G and Lagoudas D C 1994a Thermomechanical response of shape memory composites *J. Intell. Mater. Struct.* **5** 333–46

Boyd J G and Lagoudas D C 1994b A thermodynamic constitutive model for the shape memory materials. Part I. The monolithic shape memory alloys *Int. J. Plast.* submitted

Boyd J G and Lagoudas D C 1994c A thermodynamic constitutive model for the shape memory materials. Part II. The SMA composite materials *Int. J. Plast.* submitted

Brand W, Boller Chr, Huang M S and Brinson L C 1994 Introducing the constitutive behavior of shape memory alloys into adaptive engineering structures *ASME Winter Annual Meeting: Symp. on the Mechanics of Phase Transformations, and Shape Memory Alloys (Chicago, IL)*

Buehler W J and Wiley R C 1965 Nickel-base alloys *US Patent* 3,174,851

Carlson B C 1977 *Special Functions of Applied Mathematics* (New York: Academic)

Chaudhry Z and Rogers C A 1991 Bending and shape control of beams using SMA actuators *J. Intell. Mater. Syst. Struct.* **2** 581–602

Churchill S W and Chu H H S 1975 Correlating equations for laminate and turbulent free convection from a horizontal cylinder *Int. J. Heat Mass. Trans.* **18** 1049–53

de Blonk B J, Kurdila A J, Lagoudas D C and Webb G 1995 Identification of the transient response of SMA embedded flexible rods *Proc. SPIE* **2443** 349–59

Duerig T W, Melton K N, Stockel D, Wayman C M *et al* 1990 *Engineering Aspects of Shape Memory Alloys* (Butterworth-Heinemann)

Dynalloy Inc 18662 MacArthur Blvd, Suite 103, Irvine, CA 92715

Hancock H 1958 *Elliptical Integrals* (New York: Dover)

IMSL Math/Library 1990 *Fortran Subroutine for Mathematical Applications* vol 2 (IMSL)

Jackson C M, Wagner H J and Wasilewski 1972 55-Nitinol—the alloy with a memory: its physical metallurgy, properties and applications *Report* Technology Utilization Office, NASA, Washington, DC

Kakac S, Shah Ramseh K and Aung W 1987 *Handbook of Single-phase Convective Heat Transfer* (New York: Wiley)

Kreith F and Black W 1980 *Basic Heat Transfer* (New York: Harper and Row)

Lagoudas D C, Bo Z and Qidwai M A 1994 Micromechanics of active metal matrix composites with shape memory alloy fibers *Inelasticity and Micromechanics of Metal Matrix Composites (Studies in Applied Mechanics, 41)* ed G Z Voyiadjis and J W Ju, pp 163–90

Lagoudas D C, Boyd J G and Bo Z 1994 Micromechanics of active composites with SMA fibers *ASME J. Mater. Sci. Technol.* at press

Lagoudas D C and Tadjbakhsh I G 1992 Active flexible rods with embedded SMA fibers *Smart Mater. Struct.* **1** 162–7

Lagoudas D C and Tadjbakhsh I G 1993 Deformations of active flexible rods with embedded line actuators *Smart Mater. Struct.* **2** 71–81

Liang C and Rogers C A 1990 One-dimensional thermomechanical constitutive relations for shape memory materials *J. Intell. Mater. Syst. Struct.* **1** 207–34

Mayergoyz I D 1991 *Mathematical Models of Hysteresis* (New York: Springer)

McAdams W H 1954 *Heat Transmission* 3rd edn (New York: McGraw-Hill)

Morgan V T 1975 The overall convective heat transfer from smooth circular cylinders *Advanced Heat Transfer* vol 11 (New York: Academic) pp 199–264

Ortiz M and Simo J C 1986 An analysis of a new class of integration algorithms for elastophastic constitutive relations *Int. J. Num. Methods Eng.* **23** 353–66

Pfaeffle H J 1993 Active flexible rods with embedded shape memory alloy actuators: theory, design and experiment *Master's Thesis* Rensselaer Polytechnic Institute, Troy, New York, USA

Pfaeffle H J, Lagoudas D C and Craig K C 1993 Design of flexible rods with embedded SMA actuators *Proc. SPIE* **1917** 762–73

Press W H *et al* 1986 *Numerical Recipes* (Cambridge: Cambridge University Press)

Rhee S W and Koval L R 1993 Comparison of classical control with robust control for SMA smart structures *Smart Struct. Intell. Syst.* **1917** 819–33

Rogers C, Liang C and Barker D 1989 Behavior of shape memory alloy reinforced composite plates (part I and II) *Proc. 30th Structures, Structural Dynamics and Materials Conf. (Mobile, Alabama, 1989)*

Tadjbakhsh I G and Lagoudas D C 1994 Variational theory of motion of curved, twisted and extensible elastic rods *Int. J. Eng. Sci.* **32** 569–77

Tanaka K 1986 A thermomechanical sketch of shape memory effect: one-dimensional tensile behavior *Res Mechanica* **18** 251–63

Xu G, Shu S G and Lagoudas D C 1995 Thermo-electro-mechanical modeling and structural response of a flexible beam with external SMA actuators *Proc. SPIE* **2442** 503–10

Zuiker J R and Dvorak G J 1994a On the effective properties of functionally graded composites-I. Extension of the Mori–Tanaka method to linearly varying fields *Composites Eng.* **4** 19–35

Zuiker J R and Dvorak G J 1994b On the effective properties of composite materials by the linearly field *ASME J. Eng. Mater. Technol.* **116** 428–37